Evidence of Nucleation Flames: A Valuable Tool for the Study of Soot Particles Inception

T. Mouton, X. Mercier*, P. Desgroux

PC2A, CNRS/Université de Lille, France

Abstract

In this paper, we discuss the possibilities of stabilising "nucleation" flames, that is, rich flames generating soot particles for which surface growth processes are not observed. The experimental conditions for these flames are in this work determined by laser induced incandescence (LII) measurements. We also report the concentration profiles of naphthalene and two mass isomers, the pyrene and fluoranthene, measured by jet cooled laser induced fluorescence (JCLIF) in both "standard" sooting flame (with soot growth) and in a nucleation flame. From the following discussion, we highlight the interest of using this kind of flame as a valuable tool for the comprehension of the soot particles inception.

Introduction

The understanding of soot formation mechanisms in flames, and more specifically the nucleation process, is still under debate. To deal with this crucial step, low pressure laminar flames are particularly well suited because of the large reaction zone provided by the low pressure which offers the ability to spatially resolve the very early soot formation zone. The number of soot particles is however much lower than at atmospheric pressure which requires therefore sensitive techniques to be implemented in order to get accurate data.

This work presents some results of the study we carried out on the formation of soot particles in premixed $CH_4/O_2/N_2$ flames done by jet cooled laser induced fluorescence (JCLIF) and laser induced incandescence (LII). Flames were stabilised at 26.6 kPa (200 torr). In this paper, we report t he experiments we make for two different equivalence ratios (Φ = 1.95 and 2.32). Φ = 1.95 corresponds to the equivalence ratio for which LII signals begin to be measurable along the flame.

We specifically took advantage of the low-pressure conditions to probe with a good spatial resolution the soot inception zone of the flames. Mole fraction profiles of three PAHs including naphthalene and two mass isomers, pyrene and fluoranthene, have been determined in these flames. Significant differences between the evolution of the profiles of the Φ = 1.95 flame and the Φ = 2.32 are observed. The evolution of the intensity of the LII signals with the laser energy (fluence curves) is reported for different heights above the burner (HAB).

As discussed in the following, these experiments highlight the possibilities of generating nucleation flames, that is, flames which generate particles experiencing only very weak or even no surface growth.

1. Experiment Setup

1.1 Flame apparatus

The flat-flame burner (6 cm diameter) we used, provided by *Holthuis & Associates*, has been described previously [1,2]. Measurements of PAHs and soot particles have been carried out in different methane flames diluted with nitrogen. The flame conditions are reported in table 1. All these flames were considered as sooting flames featuring a yellow colour characteristic of the soot particles.

Φ	1.95	2.05	2.15	2.32
C/O	0.49	0.51	0.54	0.58
X_{CH4}	42.5%	43.0%	44.6%	46.2%
X_{O2}	43.5%	42.0%	41.4%	39.8%
X_{N2}	14.0%	15.0%	14.0%	14.0%

Total flow rate: 3.96 L/min STP

Table 1: Flames conditions

1.2 LII Setup

A schematic of the LII setup is reported in fig.1.

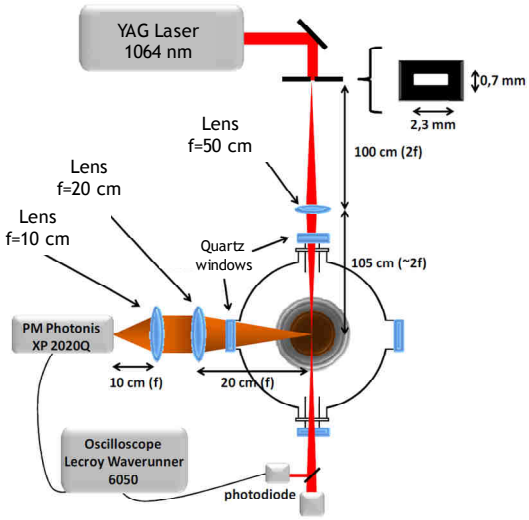

Figure 1: Experimental LII Setup

* Corresponding author: xavier.mercier@univ-lille1.fr

LII experiments were carried out directly inside the flame by using a Nd:YAG laser (Quantel 781C) to heat the soot particles [3]. The radial irradiance profile of the beam has been transformed into a top hat energy profile by the use of a rectangular slit (0.7mm x 2.3mm) and a converging lens (f=1 m). The energy of the laser beam could be adjusted thanks to an optical attenuator and was monitored with a power meter after the output window. Reflective losses were taken in account. LII signals were recorded at 90° from the incident beam thanks to a two-achromatic-lenses collecting system. The vertical spatial resolution of the LII measurements inside the flame was achieved with a horizontal slit (0.1mm x 0.5mm) parallel with the laser beam and placed in front of a UV-visible PMT (photonis XP 2020Q, spectral range 150–650 nm and maximum sensitivity around 420 nm). Signals from the PMT were acquired and digitized by an oscilloscope (Lecroy WaveRunner 6050, 500MHz bandwidth, 5GS/s sampling rate).

1.3 JCLIF Setup

A schematic representation of the setup is reported in fig.2.

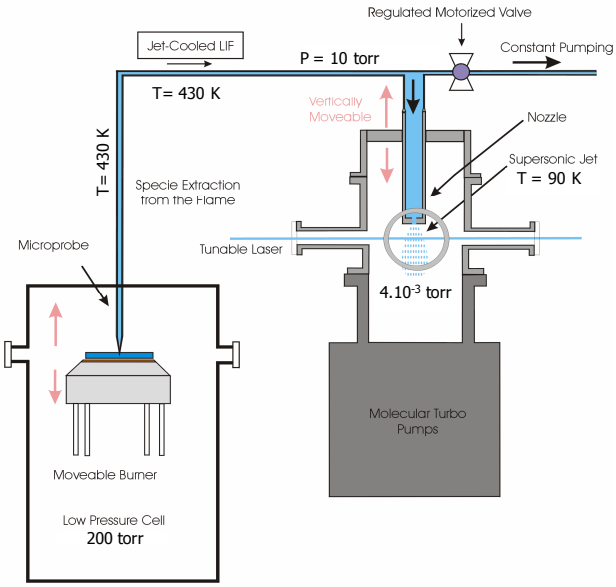

Figure 2: Experimental JCLIF Setup

JCLIF experiments were carried out after the sampling of the species from the flame thanks to an axially-oriented microprobe which was a thin quartz tube (6 mm diameter) ended by a 20° conical aperture with a diameter of 300 µm. Then species are directly cooled down in the expanded free jet generated inside the analysis chamber. LIF measurements were done directly in the free jet in this low pressure chamber. By this way, spectra of sampling PAHs highlight specific spectral structures which enable their selective measurement by LIF. In the absence of collision inside the free jet, LIF signal can be calibrated by studying the LIF signal issued from pure compounds with known concentrations sent and cooled down inside the free jet. The laser system we used consisted of a Quantel Nd:YAG laser, pumping a dye laser (TDL70 Quantel) with the 2nd harmonic at 532 nm. Tuneable wavelengths covering different spectral ranges could be generated by using different dyes to match the spectral excitation range of the three studied PAHs. The laser beam was spatially reduced to a diameter of approximately 2 mm with a pinhole and sent into the analysis chamber, slightly focused with a converging lens (500 mm focal lens). The laser energy was adjusted around 0.012-0.024 J/cm² to be in the linear regime of fluorescence. Fluorescence emission spectra were recorded via a spectrometer Acton 2500i, equipped with a 300 gr/mm grating, which could be either coupled to a 16 bit intensified CCD camera (Roper Pimax II) or to the photomultiplier (Photonis XP2020Q) described previously. The conditions of excitation and collection wavelengths for the measurement of the different PAHs are reported in table 2.

	Naphthalene	Pyrene	Fluoranthene
Transition	$S_1 \leftarrow S_0$	$S_2 \leftarrow S_0$	$S_4 \leftarrow S_0$
Excitation	λ_{ex}=307.6 nm	λ_{ex}=321 nm	λ_{ex}=319 nm
Collection	320< λ_{ex}<340	370< λ_{ex}<390	430< λ_{ex}<450

Table 2: Spectroscopic data

2. Results and discussion

LII experiments have been carried out in the two different equivalence ratio flames defined in table 1. As discussed in details in a recent review [4], the LII emission intensity is defined as $I_{LII,\lambda} = K_\lambda^a B(T,\lambda) w_{\text{laser}}$, where $B(T,\lambda)$ is the Planck function, w_{laser} is the width of the laser sheet, and K_λ^a is defined as the absorption coefficient $K_\lambda^a = N_p \pi^2 d_p^3 E(m_\lambda)/\lambda$, where N_p is the number density of primary particles, d_p the soot particle diameter, λ is the measurement wavelength and $E(m_\lambda)$ is a light absorption function of the complex refractive index of soot m_λ. K_λ^a scales linearly with f_v as $f_v = K_\lambda^a \lambda / \left(6\pi E(m_\lambda)\right)$ and the rate of signal decay scales with the active area for conductive cooling which correlates with d_p [5]. In fig.3 are reported the evolution of the temporal LII signals we measured for different heights above the burner for the two different equivalence ratios.

In the richest flame, we can deduce from these experiments that the LII signal can be correlated to three different regions. A first region, ranging from 11 to 16 mm corresponding to a zone where the temporal LII decays do not evolve with the height above the burner. We therefore assign this area to the nucleation zone of the flame. After this zone, we clearly observe an increase of the temporal decays of the LII signal, from 16 to 36 mm. These measurements gives thus evidence of a growing zone of the soot in this part of the flame, where coalescence and coagulation processes as well as surface reactions could take place. Finally, we can define a last region from 36 up to 44 mm above the burner, where the temporal LII decay curves do not

evolve anymore. This last zone could be ascribed to the aggregation region of the flame.

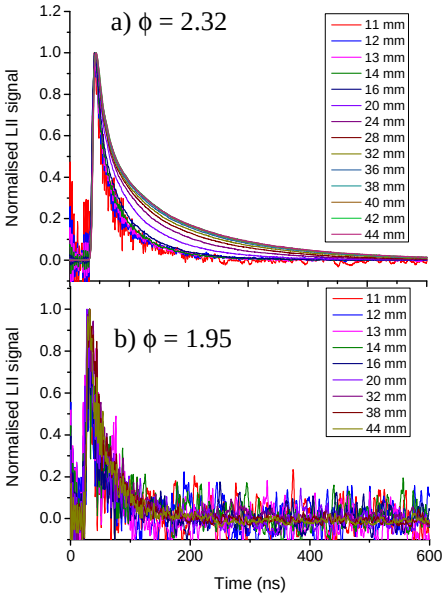

Figure 3: LII temporal decays measured at different HAB (inset) for the two equivalent ratio flames. Peak LII signals have been normalised to 1. Laser fluence set at 0.2 J/cm^2

By comparison with this flame, we do not observe in fig.3.b such an evolution of the LII decays curves measured in the $\phi = 1.95$ flame. In this flame, the temporal signals are similar all along the flame height. The absence of any increase of the LII temporal signals, gives thus evidence that growth reaction process are absent in this flame, indicating that only nucleation process would seem to take place at this equivalence ratio.

To explore deeper these results, we carried out the determination of the LII fluence curves for different heights above the burner in both flames. These fluence curves correspond to the measurement of the maximum intensities of the LII signals according to the laser fluence. The results we get are reported in fig.4.

Regarding the fig.4.a corresponding to the $\phi = 2.32$ flame, we clearly denote an evolution of the shape the fluence curve with the height above the burner. Hence, for the highest region of the flame (measurements done above 30 mm), we obtain a standard "S" shape curve characterised by a maximum value around 0.2 J/cm^2 followed by a decrease of the signal intensities featuring the sublimation of the soot particles. This shape is similar to the shape of fluence curves measured in atmospheric sooting flames for mature soot.

However, the shape of the fluence curves measured in the region we assigned to the nucleation region is very different. Indeed, we observe that in this zone, the fluence curves are characterised by quasi-linear evolution with the laser energy. This shape also means that these nascent particles could not be sublimated even at the highest available laser energies.

The evolution of the shape of the fluence curves denotes therefore a sensible evolution of the light absorption function $E(m_\lambda)$ according to the height above the burner correlated with the evolution of the physicochemical properties of the soot particles according during the soot formation process. This last point is coherent with the fact that nascent soot are expected to highlight different optical properties from those of mature soot.

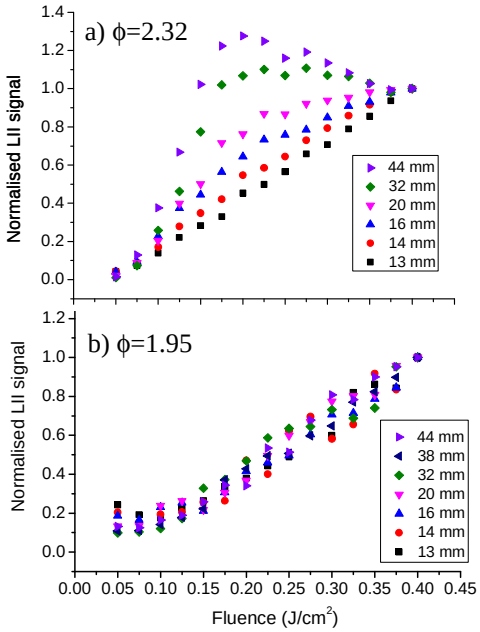

Figure 4: LII signal versus laser fluence (fluence curves) normalised to 1 for 0.4 J/cm^2 the two equivalent ratio flames

Concerning the $\phi = 1.95$ flame whose experiments are reported in fig.4.b, we denote very similar shape of fluence curves for whatever the heights above the burner, characterised by a quasi-linear dependence with the laser energy. We also remark that the particles in this flame could not reach the sublimation threshold for any height above the burner as it was the case in the nucleation region of the $\phi = 2.32$ flame. Very interestingly, the value of the slope characterising the linear fluence curves in the nucleation zone of the richest flame is the same as the one we obtain in the $\phi = 1.95$ flame.

Therefore, we denote a strong similarity between the response to the laser heating of the soot particles formed in the $\phi = 1.95$ flame and in the nucleation region of the $\phi = 2.32$ flame. This comparison clearly indicate some similarities of the physicochemical properties of the nascent soot of the richest flame with the soot of the $\phi = 1.95$ which lead us to consider this last flame as a nucleation flame, i.e., a flame where only nucleation processes take place. Note that this kind of flame is not fuel dependent and can also be stabilised at atmospheric pressure. We have recently reported in a paper a study concerning a nucleation ethylene/air flame stabilised at

atmospheric pressure highlighting the same kind of properties [6].

In order to explore deeper the specificities of the nucleation flame, we have also recorded the mole fraction profiles of soot particles as well as three different PAHs in both flames. Note that LII profiles have been calibrated in soot volume fraction profile thanks to extinction measurements carried out by cavity ring down spectroscoscopy (CRDS) [7]. Mole fraction profiles of naphthalene, pyrene and fluoranthene and soot volume fraction profiles we obtained are reported in fig.5 for the ϕ = 2.32 flame and fig.6 for the ϕ = 1.95 flame.

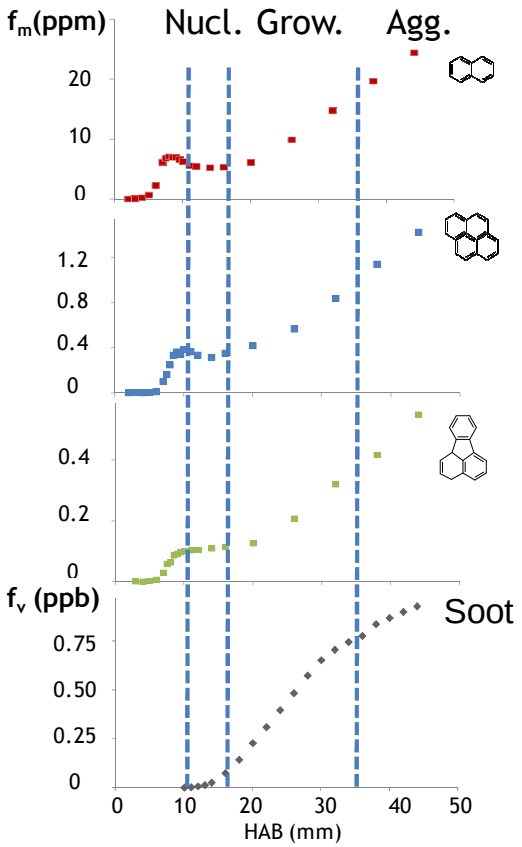

Figure 5: Mole fraction profiles PAHs and soot volume fraction profiles measured in the ϕ = 2.32 flame.

The three different regions of the flame, defined according to the LII temporal decays measurements have been plotted in both figures 5 and 6. They correspond to the three different steps of the soot formation processes, i.e. nucleation, surface growth, aggregation.

We observe that, in both flames, the nucleation region of the soot particles appears just after the peak of the maximum concentrations of PAHs. For the ϕ = 2.32 flame, this region is characterised by a slight decrease of the PAHs concentration followed by a plateau along the few millimetres assigned to the nucleation zone. After this zone, PAHs concentration profiles are marked by a strong re-increase in the growing zone. We also observe an increase of the slope of the soot mole fraction profile in this zone of the flame. Finally, the last part of the soot volume fraction profile is marked by a slight change of the slope of the profile, highlighting a diminution of the soot formation rate in the zone defined as the aggregation region.

Concerning the ϕ = 1.95 flame, we assign its whole area as a nucleation region, which is reported in fig.6, as we did not observed any evidence of soot growth in this flame according to the LII experiments. We can first note the shape of the PAHs profiles is very different from the ones determined in the ϕ=2.32 flame. Especially pyrene and fluoranthene profiles do not highlight any strong re-increase of concentration in the burnt gases but are characterised by a barely constant value following an initial increase of concentration before the soot inception. Again, we observe a good correlation between the beginning of the soot formation and the peak of the PAHs concentration profiles. The soot mole fraction profile is characterised by a continuous increase all along the flame, but we do not observe any evident break of slope as it was the case for the growing zone defined in the ϕ = 2.32 flame.

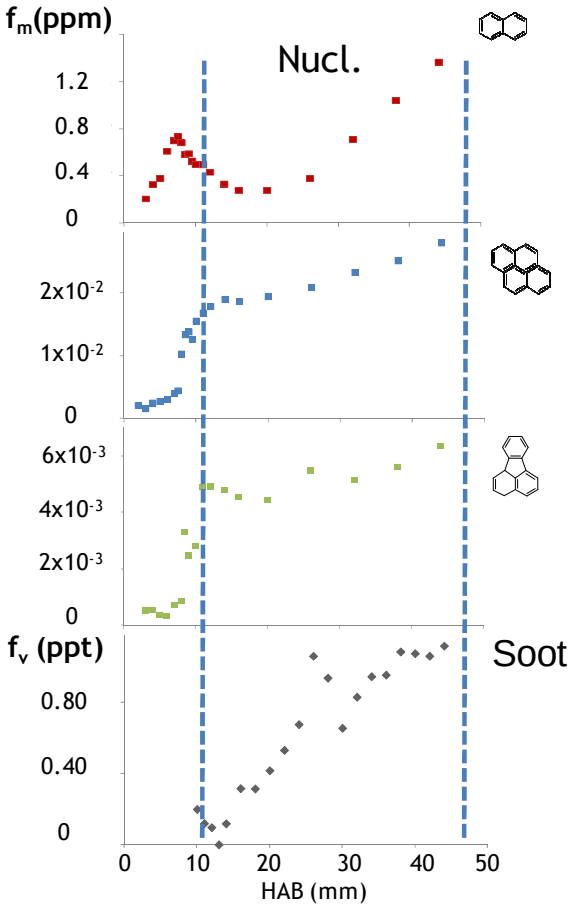

Figure 6: Mole fraction profiles PAHs and soot volume fraction profiles measured in the ϕ = 2.32 flame.

An interesting point regarding these experiments is the similarity of the evolution of the pyrene and

fluoranthene profiles in the nucleation region between the two flames. Indeed, one can note that the concentration profiles of these compounds measured in the $\phi = 1.95$ flame appears as an enlargement of the concentration profiles of the same species measured in the nucleation region of the $\phi = 2.32$ flame. The concentration profiles in both cases are characterised by a quasi-stationary state meaning that reactions of consumption and formation of these species balance each other in this part of the flames. This observation is to be explored more deeply, especially because we have not yet measured the temperature profiles for these flames which can be of importance to explain the shape of these profiles.

The soot volume fraction profiles increase all along the flame in both cases. . From the definition of f_v given in section 3, the increase of the soot mole faction can be related to the increase of the soot number particles and the soot diameter. Concerning the $\phi = 1.95$ flame, we showed, from the determination of the temporal LII decay signals and the corresponding fluence curves that there was no diameter increase all along the flame height. Therefore, the increase of the soot volume fraction in this flame can only be related to the increase of the number of particles due to the nucleation process. By comparison, in the $\phi = 2.32$ flame, the soot increase may be mainly attributed to the soot growth as shown in [3].

Regarding all these points, this flame, we defined as a “nucleation” flame, could certainly be of great interest for the study of the nucleation process which currently is the main grey area for the comprehension of the soot formation processes. This kind of flame, characterised by the absence of any surface growth reactions or growing processes as coagulation or coalescence, allows great simplification for the development of soot formation models. The parameter α corresponding to the fraction of reactive soot surface available for reactions, which is a difficult parameter to estimate, can be neglected here as there is no need to care about the growth of particles by surface reactions as the increase of the soot concentration is only due the increase of the number of particles. Hence, all these simplifications provide some evident facilities that could really profit to the developments of soot models and more specifically the understanding of the nucleation process.

3. Conclusion

In this work we have reported evidences of the existence of nucleation flames, which are rich flames characterised by the formation of soot particles which are not subject to growth processes. Concentration profiles of three different PAHs and corresponding soot volume fraction have been reported in two different flame, a reference flame ($\phi = 2.32$) and the so called nucleation flame ($\phi = 1.95$).

Concerning the PAHS, although we did not measure yet the temperature profiles, they seem to be well correlated to the different nature of the flames. All PAHs profiles are characterised by maximum values just before the beginning of the inception of soot particles. Moreover, the shape of the pyrene and fluoranthene profiles, which are potentially PAHs that could be responsible of the nucleation, are characterised by a quasi-stationary state indicating a equilibrium between the formation and consumption reaction rates both in the nucleation region of the $\phi = 2.32$ flame and in the nucleation flame.

Finally, different experiments have been carried out by LII in order to characterise the soot particles. From these experiments, it appears that in both flames, we observe a growing of the soot mole faction f_v with the height above the burner. However, the growing of f_v in the nucleation flame has been shown to be only due to the increase of the number of particles. We believe that this point could represent an important simplification for the development of soot formation model and that nucleation flames could be used as valuable tools for experimental and modelling studies with the aim of elucidating the soot nucleation processes.

Acknowledgments:

This work was supported by the Air Quality Program of CPER-IRENI (Institut de Recherche en ENvironnement Industriel) and the Labex CaPPA through the Programme d'Investissement d'Avenir (ANR-11-LABX-005-01).

References:

1. X. Mercier; M. Wartel; J. F. Pauwels; P. Desgroux, *Applied Physics B: Lasers and Optics* **2008,** 91, (2), 387-395.
2. M. Wartel; J. F. Pauwels; P. Desgroux; X. Mercier, *Applied Physics B: Lasers and Optics* **2010,** 100, (4), 933-943.
3. T. Mouton; X. Mercier; M. Wartel; N. Lamoureux; P. Desgroux, *Applied Physics B: Lasers and Optics* **2013**, 1-11.
4. P. Desgroux; X. Mercier; K. A. Thomson, *Proceedings of the Combustion Institute* **2013,** 34, (1), 1713-1738.
5. C. Schulz; B. F. Kock; M. Hofmann; H. Michelsen; S. Will; B. Bougie; R. Suntz; G. Smallwood, *Applied Physics B: Lasers and Optics* **2006,** 83, (3), 333-354.
6. H. Bladh; N.-E. Olofsson; T. Mouton; J. Simonsson; X. Mercier; A. Faccinetto; P.-E. Bengtsson; P. Desgroux, *Proceedings of the Combustion Institute* **2015,** 35, (2), 1843-1850.
7. P. Desgroux; X. Mercier; B. Lefort; R. Lemaire; E. Therssen; J. F. Pauwels, *Combustion and Flame* **2008,** 155, (1-2), 289-301.